Direct Observation of Continuous Electric Dipole Rotation in Flux-Closure Domains in Ferroelectric Pb(Zr,Ti)O_3

Chun-Lin Jia, *et al.*

Science **331**, 1420 (2011);
DOI: 10.1126/science.1200605

This copy is for your personal, non-commercial use only.

If you wish to distribute this article to others, you can order high-quality copies for your colleagues, clients, or customers by clicking here.

Permission to republish or repurpose articles or portions of articles can be obtained by following the guidelines here.

The following resources related to this article are available online at www.sciencemag.org (this infomation is current as of October 17, 2011):

Updated information and services, including high-resolution figures, can be found in the online version of this article at:
http://www.sciencemag.org/content/331/6023/1420.full.html

Supporting Online Material can be found at:
http://www.sciencemag.org/content/suppl/2011/03/16/331.6023.1420.DC1.html

This article **cites 31 articles**, 4 of which can be accessed free:
http://www.sciencemag.org/content/331/6023/1420.full.html#ref-list-1

This article appears in the following **subject collections:**
Materials Science
http://www.sciencemag.org/cgi/collection/mat_sci
Physics
http://www.sciencemag.org/cgi/collection/physics

Downloaded from www.sciencemag.org on October 17, 2011

Science (print ISSN 0036-8075; online ISSN 1095-9203) is published weekly, except the last week in December, by the American Association for the Advancement of Science, 1200 New York Avenue NW, Washington, DC 20005. Copyright 2011 by the American Association for the Advancement of Science; all rights reserved. The title *Science* is a registered trademark of AAAS.

10. M. J. Drake, H. E. Newsom, C. J. Capobianco, *Geochim. Cosmochim. Acta* **53**, 2101 (1989).
11. M. J. Walter, H. E. Newsom, W. Ertel, A. Holzheid, in *Origin of the Earth and Moon*, R. M. Canup, K. Righter, Eds. (Univ. of Arizona Press, Tucson, AZ, 2000), pp. 265–289.
12. A. S. Ellis, T. M. Johnson, T. D. Bullen, *Science* **295**, 2060 (2002).
13. F. Moynier, Q. Z. Yin, B. Jacobsen, *Lunar Planet. Sci. Conf.* **38**, 1406 (2007).
14. R. Schönberg, S. Zink, M. Staubwasser, F. von Blanckenburg, *Chem. Geol.* **249**, 294 (2008).
15. Materials and methods are available as supporting material on *Science* Online.
16. We define the Cr isotopic fractionation per atomic mass unit as δCr/amu = $\delta^{50/52}$Cr/(–2), where $\delta^{50/52}$Cr is parts per thousand deviation in ^{50}Cr/^{52}Cr of the sample relative to the Cr standard SRM 979 (*15*). Literature data for Cu and Zn isotopes were treated similarly as δCu/amu (*20*) and δZn/amu (*21*).
17. F. Moynier, F. Albarede, G. Herzog, *Geochim. Cosmochim. Acta* **70**, 6103 (2006).
18. F. Moynier *et al.*, *Earth Planet. Sci. Lett.* **277**, 482 (2009).
19. F. Moynier *et al.*, *Chem. Geol.* **276**, 374 (2010).
20. J. M. Luck, D. B. Othman, J. A. Barrat, F. Albarede, *Geochim. Cosmochim. Acta* **67**, 143 (2003).
21. J. M. Luck, D. B. Othman, F. Albarede, *Geochim. Cosmochim. Acta* **69**, 5351 (2005).
22. R. N. Clayton, T. K. Mayeda, *Geochim. Cosmochim. Acta* **63**, 2089 (1999).
23. C. Fitoussi, B. Bourdon, T. Kleine, F. Oberli, B. C. Reynolds, *Earth Planet. Sci. Lett.* **287**, 77 (2009).
24. R. Chakrabarti, S. Jacobsen, *Geochim. Cosmochim. Acta* **74**, 6921 (2010).
25. E. Schauble, G. R. Rossman, H. P. Taylor Jr., *Chem. Geol.* **205**, 99 (2004).
26. B. J. Wood, *Philos. Trans. R. Soc. London Ser. A* **366**, 4339 (2008).
27. A. Corgne, S. Keshav, B. J. Wood, W. F. McDonough, Y. Fei, *Geochim. Cosmochim. Acta* **72**, 574 (2008).
28. Y. Ricard, O. Sramek, F. Dubuffet, *Earth Planet. Sci. Lett.* **284**, 144 (2009).
29. J. Monteux, Y. Ricard, N. Coltice, F. Dubuffet, M. Ulvrova, *Earth Planet. Sci. Lett.* **287**, 353 (2009).
30. T. W. Dahl, D. J. Stevenson, *Earth Planet. Sci. Lett.* **295**, 177 (2010).
31. J. F. Rudge, T. Kleine, B. Bourdon, *Nat. Geosci.* **3**, 439 (2010).
32. R. N. Clayton, *Nature* **415**, 860 (2002).
33. H. Yurimoto, K. Kuramoto, *Science* **305**, 1763 (2004).
34. J. R. Lyons, E. D. Young, *Nature* **435**, 317 (2005).
35. A. Trinquier, J.-L. Birck, C. J. Allègre, *Astrophys. J.* **655**, 1179 (2007).
36. Q. Z. Yin *et al.*, *Lunar Planet. Sci. Conf.* **40**, 2006 (2009).
37. F. Moynier *et al.*, *Astrophys. J.* **718**, L7 (2010).
38. G. W. Kallemeyn, J. T. Wasson, *Geochim. Cosmochim. Acta* **45**, 1217 (1981).
39. K. Lodders, B. Fegley Jr., *The Planetary Scientist's Companion* (Oxford Univ. Press, Oxford, 1998).
40. Y. Wang, W. B. Hsu, *Meteorit. Planet. Sci.* **44**, 763 (2009).

41. We acknowledge NASA funding (LASER grant NNX09AM64G to F.M. and Cosmochemistry grant NNX08AG57G and Origins of Solar Systems grant NNX09AC93G to Q.-Z.Y.) and NSF funding (grants EAR0643286 and EAR0711411 to E.S.). We thank B. Jacobsen for his assistance in the laboratory; J. Wasson, A. Rubin, and J. Wimpenny for helpful discussions; and two reviewers for their insightful and constructive comments.

Supporting Online Material

www.sciencemag.org/cgi/content/full/science.1199597/DC1
SOM Text
Tables S1 to S5
References

26 October 2010; accepted 1 February 2011

10.1126/science.1199597

Direct Observation of Continuous Electric Dipole Rotation in Flux-Closure Domains in Ferroelectric Pb(Zr,Ti)O_3

Chun-Lin Jia,[1]* Knut W. Urban,[1] Marin Alexe,[2] Dietrich Hesse,[2] Ionela Vrejoiu[2]

Low-dimensional ferroelectric structures are a promising basis for the next generation of ultrahigh-density nonvolatile memory devices. Depolarization fields, created by incompletely compensated charges at the surfaces and interfaces, depress the polarization of such structures. Theory suggests that under conditions of uncompensated surface charges, local dipoles can organize in flux-closure structures in thin films and vortex structures in nano-sized ferroelectrics, reducing depolarization fields. However, the continuous rotation of the dipoles required in vortex structures and the behavior of unit cell dipoles in flux-closure structures have never been experimentally established. By aberration-corrected transmission electron microscopy, we obtained experimental evidence for continuous rotation of the dipoles closing the flux of 180° domains in a ferroelectric perovskite thin film.

Ferroelectric thin films have demonstrated great potential for microelectronics applications (*1*–*5*). In ferroelectric random access memories, information is stored and read by switching and detecting the polarization orientation in the ferroelectric material. Microscopically, polarization switching is realized through the motion of domain walls driven by an external electric field. Phenomenologically, domain arrangements are characterized by the angle between polarization directions in adjacent domains. Stripes of 180° domains have been reported for thin films of $PbTiO_3$ on $SrTiO_3$ (*6*, *7*). In epitaxial thin-film systems, the domain pattern is determined by the growth conditions and by the mechanical interface strain and the electric boundary conditions related to the depolarization field at surfaces or interfaces. Ideally, two such boundary conditions can be distinguished according to whether the surface or interface charges are perfectly screened (e.g., by conducting electrodes) or unscreened (vacuum or insulating surface layers). In addition, the effect of anisotropic electrostriction must be considered. It imposes a substantial energy cost for rotating the polarization away from the normal symmetry-allowed lattice directions. Theoretical studies on $Pb(Zr_{1-x}Ti_x)O_3$ have revealed a variety of different domain patterns depending on the competition between these factors. Nonetheless, theory predicts as a general feature the formation of a stripe-type pattern of Landau-Lifshitz polarization with 90° flux-closure structures at surfaces or interfaces, whereby the strength of the depolarization field is reduced (*8*–*11*). Flux-closure structures in ferroelectric materials are currently a subject of intensive interest. Recent experiments reported their existence at the junctions of multiple 71° or 90° domains (*12*, *13*). Flux-closure structures, which were predicted by theory in ferroelectric film systems with 180° stripe domains, have not yet been corroborated by experiment.

Theoretical investigations have shown that in very small ferroelectric structures a few nanometers in size, the local dipoles should organize in vortices rather than in domains with uniform polarization because of the large depolarization fields (*14*, *15*). Experimental results have been reported for $Pb(Zr_{0.4}Ti_{0.6})O_3$, $Pb(Zr_{0.3}Ti_{0.7})O_3$, $BaTiO_3$ nanodots, and fine-grained polycrystalline samples; these have been interpreted in terms of vortex structures (*16*–*18*). However, the spatial resolution of these studies was too low to provide direct evidence for the formation of a vortex phase. Recently, Nelson *et al.* reported on observations by aberration-corrected scanning transmission electron microscopy (STEM) of vortex-like nanodomain arrays at 109° domain walls at the interface in $BiFeO_3$ films grown by molecular beam epitaxy on $TbScO_3$ substrates (*19*). A vertical 109° domain wall splits into a mirrored pair of inclined 180° domain walls and a 109° wall of opposite sense. In this way a vortex domain structure is formed, with the polarization rotating about the intersection of two 109° and two 180° domain walls. This complex domain wall arrangement, together with the interface epitaxy constraints, leads to a local broadening of the walls, which makes the polarization rotation quasi-continuous. Although insufficient resolution prevents the accompanying phase-field simulations from reproducing this quasi-continuous rotation, they show that for this particular material combination, such a multidomain arrange-

---

[1] Peter Grünberg Institute and Ernst Ruska Center for Microscopy and Spectroscopy with Electrons, Forschungszentrum Jülich, D-52425 Jülich, Germany. [2] Max Planck Institute of Microstructure Physics, Weinberg 2, D-06120 Halle, Germany.

*To whom correspondence should be addressed. E-mail: c.jia@fz-juelich.de

ment corresponds to a low-energy situation that minimizes depolarization.

The observations described below, in addition to giving evidence of the existence of flux-closure structures at a 180° domain wall, represent a direct experimental proof of continuous polarization rotation on the atomic scale. Using atomic-resolution aberration-corrected TEM, we studied domain structures of the epitaxial thin-film system $PbZr_{0.2}Ti_{0.8}O_3$ (henceforth PZT) on $SrTiO_3$ (STO) (*20*). We made use of the negative spherical aberration imaging (NCSI) technique, which allows not only location of all the atomic species but also measurement of their positions, unit cell by unit cell, with a precision of a few picometers (*21*–*24*). On this basis we calculated the relative ion displacement and the electric dipole moment for the individual unit cells. The resulting map of dipole moments depicts the atomic morphology of domains and domain walls. In this way we identify a near-interface region within the PZT film where the local dipoles rotate continuously, forming a flux-closure structure connecting two 180° domains.

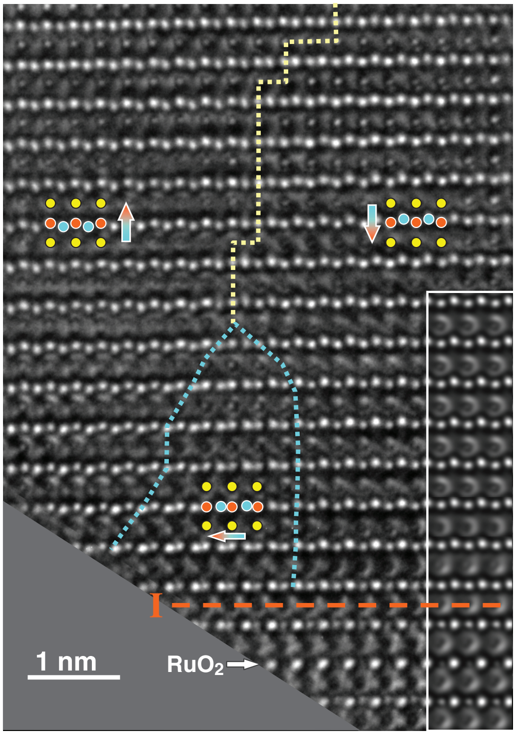

Fig. 1. Atomic-resolution image of a flux-closure structure with continuous dipole rotation in $PbZr_{0.2}Ti_{0.8}O_3$ (PZT) close to the interface to the $SrTiO_3$ (STO) substrate. The interface is marked by a horizontal dashed line (I), which is determined on the basis of a $SrRuO_3$ marker layer with a nominal thickness of 1.5 unit cells at the STO-PZT interface. The RuO_2 marker layer is also indicated. In the image recorded along the crystallographic [$\bar{1}\bar{1}0$] direction, the atomic structure and the electric dipole direction (arrows) are given. In the image, two larger domains with 180° orientation can be identified. The domain wall is indicated by a yellow dotted line. In the center of the lower half of the image, an approximately triangular area (the domain wall is indicated by a dotted blue line) can be seen, where in the center the dipole direction makes an angle of 90° with the two large domains. The inset at the lower right shows a calculated image demonstrating the excellent match between the atomic model and the specimen structure.

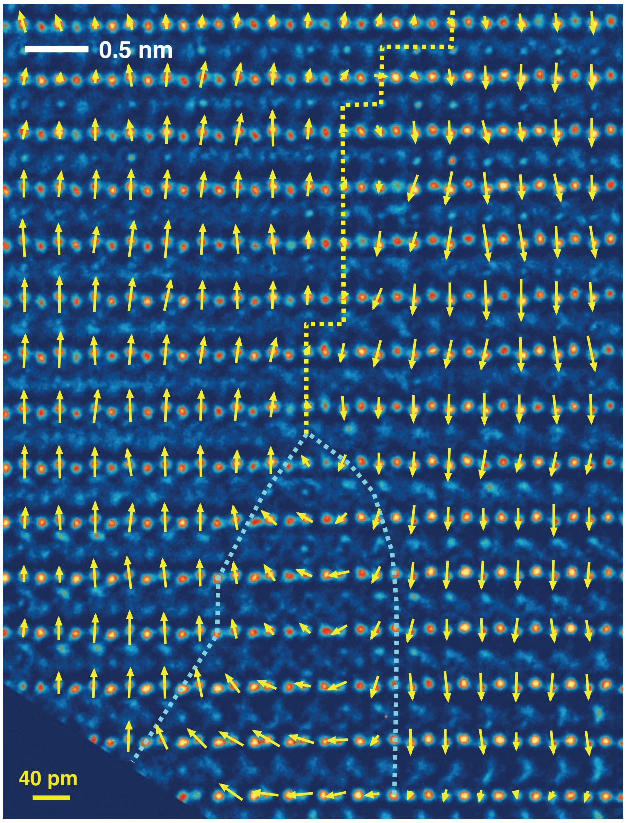

Fig. 2. Map of the atomic displacement vectors. The displacement of the Zr-Ti atoms (arrows) from the center of the projected oxygen octahedra is shown here superposed on the atomic image of Fig. 1. To enhance contrast, the gray scale is converted into a false-color representation. The length of the arrows represents the modulus of the displacements with respect to the yellow scale bar in the lower left corner. The arrowheads point into the displacement directions. Note the continuous rotation of the dipole directions from "down" (right) to "up" (left), which closes the electric flux of the two 180° domains.

Figure 1 shows an atomic-resolution image of an area including the interface between the PZT layer and the STO substrate. The arrangement of the film layers is schematically shown in fig. S1. In Fig. 1 the structure (one projected unit cell) of PZT is indicated schematically in two regions (positions of Zr-Ti, PbO-SrO, and O atomic columns, seen end-on, are indicated by red, yellow, and blue circles, respectively). Because of the particular imaging conditions, dynamic electron scattering yields a sharp bright contrast (*25*) in the ~11-nm-thick sample for the Zr-Ti and the O atom columns, whereas the SrO and PbO atomic columns are relatively weak (*20*). The film-substrate interface was marked by depositing a layer of $SrRuO_3$ (SRO), nominally 1.5 unit cells thick, on STO prior to the deposition of PZT. The interface, denoted by a horizontal dashed line, is then determined by observing the plane of RuO_2 (which serves as a marker). A quantitative contrast analysis revealed that substitutional intermixing of Ru atoms occurred into the next upper $(Zr\text{-}Ti)O_2$ and into the next lower TiO_2 plane. For reasons of symmetry, the heterostructure was capped at the upper end by a SRO layer, nominally 1.5 unit cells thick, followed by a STO layer 15 unit cells thick.

The vertical shift in the Zr-Ti positions with respect to the adjacent O positions indicates that PZT is in a polarized state. On the left side of Fig. 1, this shift is upward, whereas on the right side it is downward, resulting in the polarization vector directions indicated by the arrows. This indicates the existence of two domains in a 180° orientation relation. By mapping the individual atom shifts, the position of the domain wall (dotted line) is localized. The horizontal width of this wall is about one [$\bar{1}\bar{1}0$] projected crystal unit cell, which is in agreement with the results of earlier measurements (*22*). At the bottom interface, between the two 180° domains, in-plane displacements of the Zr-Ti positions with respect to the adjacent oxygen positions are observed. In-plane displacements have been predicted to play an important part in stabilizing such ferroelectric domain configurations (*11*).

Figure 2 displays an atomic displacement map superimposed on an image obtained by converting the grayscale contrast of Fig. 1 into a false-color scale to enhance contrast. The arrows located at the Zr-Ti column positions indicate the modulus and the direction of the "off-center"

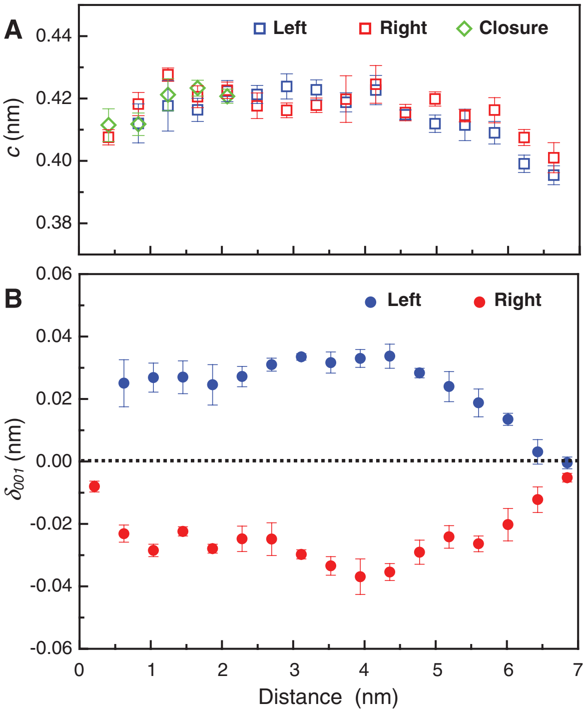

Fig. 3. (**A**) The vertical [001] lattice parameter c as a function of the distance from the lower interface. The value of c adopts a maximum value at the middle of the film layer and decreases when approaching the bottom and top interfaces. The behavior is the same in all three domain areas (red symbols for the left domain, blue for right domain, and green for flux-closure domain). (**B**) The shift parameter (δ_{001}), that is, the off-center displacements along the vertical [001] direction as a function of the distance from the lower interface. The blue symbols denote the upward displacements in the left domain; the red symbols indicate the downward displacements in the right domain. At the lower interface, the values change from the bulk value to a value close to zero within the distance of a single unit cell, whereas at the upper interface the shift parameter starts to decrease six unit cells away from the interface, reaching a value of zero there.

displacement with respect to the middle point of the horizontal line connecting the two neighboring O atom positions (taking the cubic structure with an inscribed oxygen octahedron in the nonpolar state as a reference). The scale at the lower left indicates a displacement of 40 pm. We note that a uniform atomic shift of this magnitude corresponds to an integral polarization of 108 μC/cm^2 (*22, 26*).

The displacement map provides direct evidence of a continuous rotation of the dipole direction from downward in the right-hand domain through a 90° orientation to upward in the left-hand domain, forming a particular type of flux-closure structure. The reorientation of the dipoles occurs within a well-defined area of triangular shape, with a maximum width of ~2.5 nm at the interface. The displacement vector modulus is small at the top, increasing toward the interface. The transition region from the downward orientation of the electric dipoles to the 90° orientation is about two projected unit cell widths on the right-hand side and up to about twice as wide on the left-hand side. No direct information is available on possible atom shifts along the $[\bar{1}\bar{1}0]$ viewing direction. However, the fact that we do not observe any in-plane elongation of the projected atom column contrast can be interpreted as evidence of the dipole rotation occurring exclusively in the image plane.

In Fig. 3, the [001] vertical crystal lattice parameter c and the modulus of the vertical displacements of the Zr-Ti atoms δ_{001} are displayed as a function of the distance from the STO-PZT interface to the interface at the capping STO layer (not shown in Figs. 1 and 2). The values were obtained by averaging, at a given vertical distance from the interface, the measured c values for the individual unit cells along the horizontal direction parallel to the interface. Starting (Fig. 3A) with a value of ~0.410 nm at the lower interface, c reaches a plateau value of 0.420 nm in the central part of the film layer before subsequently decreasing to 0.395 nm at the upper interface. The plateau and the upper-interface values are in good agreement with the values measured before for the fully polarized state and the depolarized state of PZT, respectively (*22*). This allows us to conclude that the presence of the flux-closure area at the lower STO-PZT interface reduces the depolarization field to such an extent that the polarization can essentially maintain its "bulk" value. On the other hand, the depolarization field at the upper interface (where we do not observe a flux-closure structure within the field of view) is so strong that polarization decays to a value close to zero. This conclusion is corroborated by the behavior of the shift parameter δ_{001} displayed in Fig. 3B. At the lower interface, both the left (upward-polarized) and right (downward-polarized) domains show a stable value on the order of 0.03 nm, typical for the polar state (*22*), down to the second horizontal atom plane (counted from the SRO marker plane). It is only in the first layer that the polarization decays. This behavior is in contrast to that in the direction to the upper interface, where δ_{001} starts to decrease six unit cells away from the interface, ultimately reaching a value of zero.

In bulk PZT, the c-axis lattice parameter and the atomic displacement of Zr-Ti and O show an equivalent behavior during the paraelectric-to-ferroelectric transition; that is, the value of both parameters increases. By contrast, we note that inside the flux-closure area, c shows the same behavior as in the adjacent domains. This means that its value is essentially unaffected by the rotation of the electric dipoles of up to 90°, which in principle should lead to a reduction of the c-axis parameter and to an expansion perpendicular to this axis (i.e., parallel to the STO-PZT interface). This behavior can be understood as a consequence of the mechanical coupling to the neighboring 180° domains, whereupon the epitaxy constraints, because of lattice parameter misfit (*27*, *28*), lead to a compressive stress in the PZT close to the interface.

Our results provide direct experimental evidence for the continuous rotation of the atomic-scale polarization dipoles over a distance directly relevant for the formation of vortex structures as predicted by theory (*14*, *15*). Our observations agree well with the results of calculations for thin-film epitaxial systems by first-principles techniques, where the lateral extension of the flux-closing area was found to be quite narrow (*8*, *10*, *29*, *30*), consistent with our own results. Furthermore, theory yields a continuous rotation of the polarization direction rather than a closure domain with a 90° polarization orientation and relatively narrow domain boundaries, as known for ferromagnetics.

The quantitative structural details of the flux-closure domain structure can be discussed in accordance with a thermodynamic theory (*31*) based on a Landau-Ginzburg-Devonshire free energy density taking into account polarization, mechanical stress, electric field, and domain wall structure. The equilibrium state, subject to consistency with Maxwell's equations and linear elasticity theory, was determined for a ferroelectric PbTiO$_3$ heterostructure comprising a substrate and capping layer of (nonconducting) STO. The result was an approximately triangular flux-closure area with a basis in the interface on the order of a few nanometers. In addition, the depolarization field was quite strong at the top interface, essentially destroying polarization in the sample, although it was rather low in the environment of the flux-closure structure. This is confirmed by our study carried out at genuine atomic resolution, permitting access to the individual elementary electric dipoles.

With respect to potential charge screening at the SRO-containing interfaces, the following is essential. For SRO, a transition from metallic-conducting to insulating has been observed at layer thicknesses below four unit cells (*32*–*34*) and two unit cells (*35*). In the present case, the nominal SRO layer thickness at the PZT-STO interface is lower than these minimum thicknesses. In addition there is evidence of chemical intermixing destroying the chemical order, which is considered important for conductivity in these reference materials. Therefore, it can be concluded that the SRO layer used as a marker for the interface position is nonmetallic and thus cannot screen the depolarization field at the interface.

Continuous rotations of electric dipoles within flux-closure regions of ferroelectrics of the type observed in this work were concordantly predicted by numerous theoretical treatments. The result (*19*) on vortex-like domain structures in rhombohedral materials such as $BiFeO_3$ corroborates our observations in the epitaxial PZT-STO system. We would like to point out that the vortex-like domain structures brought about by the comparatively simple 180°-90°-180° domain arrangement of our work are observed in films of highly tetragonal $PbZr_{0.2}Ti_{0.8}O_3$, where polarization rotation might be considered less likely than in rhombohedral materials like $BiFeO_3$. Both studies show that in perovskite-oxide heterostructures, polarization-closure structures do occur. Our work demonstrates the unique capabilities of mapping of the dipole vector, unit cell by unit cell, by means of atomic-resolution TEM. This technique can therefore be used to study further details of domain structures close to interfaces in ferroelectric heterostructures and of vortex-like structures in ferroelectric materials. Because these structures are sensitive to the balance between competitive interactions, even small changes in the interface properties could have substantial effects on the depolarization field behavior. In fact, theory predicts striking effects for thicknesses on the order of a few nanometers in the PZT layer, where the top and bottom layers (metallic or insulating) cannot be treated separately (*10*). In addition, "dead" layers one unit cell thick (e.g., due to local deviations in permittivity caused by nonstoichiometry) are expected to change the flux-closure domain structure. Such investigations are also of potential importance for further progress in technology, in which increasingly thinner and smaller ferroelectric heterostructure systems are being considered for microelectronic applications.

References and Notes

1. M. E. Lines, A. M. Glass, *Principles and Applications of Ferroelectric and Related Materials* (Clarendon, Oxford, 1977).
2. J. F. Scott, *Ferroelectric Memories* (Springer, Berlin, 2000).
3. J. F. Scott, *Science* **315**, 954 (2007).
4. N. Setter, R. Waser, *Acta Mater.* **48**, 151 (2000).
5. K. Rabe, Ch. H. Ahn, J.-M. Triscone, Eds., *Physics of Ferroelectrics* (Springer, Berlin, 2007).
6. S. K. Streiffer *et al.*, *Phys. Rev. Lett.* **89**, 067601 (2002).
7. D. D. Fong *et al.*, *Science* **304**, 1650 (2004).
8. I. Kornev, H. Fu, L. Bellaiche, *Phys. Rev. Lett.* **93**, 196104 (2004).
9. B.-K. Lai, I. Ponomareva, I. Kornev, L. Bellaiche, G. Salamo, *Appl. Phys. Lett.* **91**, 152909 (2007).
10. S. Prosandeev, L. Bellaiche, *Phys. Rev. B* **75**, 172109 (2007).
11. P. Aguado-Puente, J. Junquera, *Phys. Rev. Lett.* **100**, 177601 (2008).
12. N. Balke *et al.*, *Nat. Nanotechnol.* **4**, 868 (2009).
13. L. J. McGilly, A. Schilling, J. M. Gregg, *Nano Lett.* **10**, 4200 (2010).
14. I. I. Naumov, L. Bellaiche, H. Fu, *Nature* **432**, 737 (2004).
15. I. Naumov, A. M. Bratkovsky, *Phys. Rev. Lett.* **101**, 107601 (2008).
16. A. Schilling *et al.*, *Nano Lett.* **9**, 3359 (2009).
17. B. J. Rodriguez *et al.*, *Nano Lett.* **9**, 1127 (2009).
18. Y. Ivry, D. P. Chu, J. F. Scott, C. Durkan, *Phys. Rev. Lett.* **104**, 207602 (2010).
19. C. T. Nelson *et al.*, *Nano Lett.* **11**, 828 (2011).
20. See supporting material on *Science* Online.
21. C. L. Jia, M. Lentzen, K. Urban, *Science* **299**, 870 (2003).
22. C. L. Jia *et al.*, *Nat. Mater.* **7**, 57 (2008).
23. K. W. Urban, *Science* **321**, 506 (2008).
24. C. L. Jia, L. Houben, A. Thust, J. Barthel, *Ultramicroscopy* **110**, 500 (2010).
25. M. Lentzen, *Microsc. Microanal.* **14**, 16 (2008).
26. C. L. Jia *et al.*, *Nat. Mater.* **6**, 64 (2007).
27. S. P. Alpay *et al.*, *J. Appl. Phys.* **85**, 3271 (1999).
28. I. Vrejoiu *et al.*, *Adv. Mater.* **18**, 1657 (2006).
29. B.-K. Lai *et al.*, *Phys. Rev. Lett.* **96**, 137602 (2006).
30. D. Lee *et al.*, *Phys. Rev. B* **80**, 060102(R) (2009).
31. G. B. Stephenson, K. R. Elder, *J. Appl. Phys.* **100**, 051601 (2006).
32. G. Herranz *et al.*, *Phys. Rev. B* **67**, 174423 (2003).
33. D. Toyota *et al.*, *Appl. Phys. Lett.* **87**, 162508 (2005).
34. J. Xia, W. Siemons, G. Koster, M. R. Beasley, A. Kapitulnik, *Phys. Rev. B* **79**, 140407(R) (2009).
35. Y. J. Chang *et al.*, *Phys. Rev. Lett.* **103**, 057201 (2009).

36. Supported by Deutsche Forschungsgemeinschaft grant SFB 762 (M.A., D.H., and I.V.).

Supporting Online Material

www.sciencemag.org/cgi/content/full/331/6023/1420/DC1
Materials and Methods
Fig. S1

18 November 2010; accepted 4 February 2011
10.1126/science.1200605

Vibrationally Quantum-State–Specific Reaction Dynamics of H Atom Abstraction by CN Radical in Solution

Stuart J. Greaves,[1] Rebecca A. Rose,[1] Thomas A. A. Oliver,[1] David R. Glowacki,[1] Michael N. R. Ashfold,[1] Jeremy N. Harvey,[1] Ian P. Clark,[2] Gregory M. Greetham,[2] Anthony W. Parker,[2] Michael Towrie,[2] Andrew J. Orr-Ewing[1]*

Solvent collisions can often mask initial disposition of energy to the products of solution-phase chemical reactions. Here, we show with transient infrared absorption spectra obtained with picosecond time resolution that the nascent HCN products of reaction of CN radicals with cyclohexane in chlorinated organic solvents exhibit preferential excitation of one quantum of the C-H stretching mode and up to two quanta of the bending mode. On time scales of approximately 100 to 300 picoseconds, the HCN products undergo relaxation to the vibrational ground state by coupling to the solvent bath. Comparison with reactions of CN radicals with alkanes in the gas phase, known to produce HCN with greater C-H stretch and bending mode excitation (up to two and approximately six quanta, respectively), indicates partial damping of the nascent product vibrational motion by the solvent. The transient infrared spectra therefore probe solvent-induced modifications to the reaction free energy surface and chemical dynamics.

In a chemical reaction, the partitioning of energy between translational, rotational, vibrational, and electronic degrees of freedom of the products depends on, and therefore provides information about, the potential energy landscape over which bonding changes occur (*1*). Early insights came from Polanyi (*2*), who demonstrated the importance of the location of an energy barrier along a reaction pathway in determining the fraction of the available energy that is released as product vibrational excitation. An expanding array of experimental techniques, complemented by theory, is enabling study of the dynamics of reactions in ever-increasing detail under low-pressure, gas-phase conditions in which the molecules are largely isolated from collisions and from the perturbations of a surrounding medium such as a solvent (*1*, *3*–*5*).

Much synthetic, environmental, and biological chemistry occurs in solution, however, and the solvent will have a pronounced effect on the dynamics of chemical reactions (*6*–*8*). The very short time intervals between collisions in the liquid phase, and the hindered motions of molecules surrounded by a solvent cage, prevent application of many of the velocity- and quantum-state–specific experimental methods developed to examine gas-phase collisions (*9*). Spectroscopic methods using ultrafast lasers can be used to measure the time scales for reactions in solution (*10*–*13*), study solvent-solute complexes (*14*, *15*), and examine molecular vibrational excitation, which can persist in solution for tens or hundreds of picoseconds (*16*). For a solution-phase bimolecular reaction, observation of vibrational quantum-state–specific energy disposal might provide comparable mechanistic insight to the infrared (IR) chemiluminescence (*1*, *2*) and more recent velocity-map imaging (*3*) studies of gas-phase reactions and therefore unravel the influence of the solvent on the dynamics. This prospect was recognized by Hochstrasser and co-workers (*10*, *11*), who used transient IR absorption to examine the products of reactions of Cl atoms or CN radicals with organic solvents. These pioneering experiments provided evidence that ~20% of the DCN products of the CN reaction with $CDCl_3$ solvent are formed with one quantum of vibrational excitation in the C-D stretching mode.

Here, experimental outcomes are presented for a solution-phase bimolecular reaction, which demonstrate a much greater degree of product vibra-

---

[1] School of Chemistry, University of Bristol, Cantock's Close, Bristol BS8 1TS, UK. [2] Central Laser Facility, Research Complex at Harwell, Science and Technology Facilities Council, Rutherford Appleton Laboratory, Harwell Science and Innovation Campus, Didcot, Oxfordshire, OX11 0QX, UK.

*To whom correspondence should be addressed. E-mail: a.orr-ewing@bris.ac.uk